Appendix Materials

Appendix A1: Materials and chemicals

Chemicals

All chemicals were of analytical reagent except acetonitrile, tetrahydrofuran and methanol as these were HPLC grade. The chemicals used in this study were purchased from Tianjin Damao Chemical Agent Company (Tianjin, China) except BDE209 (98%, purchased from Aladdin Shanghai, China). All chemicals were used as received without further purification.

Biochar-supported nZVI particles synthesis details

For BC@nZVI, 0.1 M $FeSO_4 \cdot 7H_2O$ was prepared in 100 mL ethanol/water (30/70, v/v) with an appropriate amount of PVP (nZVI/PVP, w/w = 1/1) and then mixed with a defined amount of biochar by mechanical agitation for 1 h to completely mix the solution. 50 mL of 0.3 M $NaBH_4$ solution was added dropwise to reduce Fe^{2+} to Fe^0 and the mixture was stirred until no significant H_2 production was observed. Subsequently, the black particles formed were magnetically separated and washed three times with deionized water to remove the excess $NaBH_4$. Then, the solids were washed several times with respectively ethanol and acetone and finally vacuum dried at 60℃.

Soil collection and preparation

The soil used in this study was obtained from the Guangzhou, Guangdong province (China) and the physicochemical properties of the soil are listed in Table S1. The soil was artificially contaminated using our previously reported method (Wu et al., 2016).

Appendix A2: Analysed and Experiment

Analysed detailed

The N_2 Brunnaer–Emmett–Teller (BET) surface area analyses of the synthesized particles were performed using an ASAP2020M surface analyzer (Micromeritics Instruments, USA). The surface Zeta-potential and hydrodynamic diameter of the materials were measured by Zetasizer Nano ZS90 instrument (Malvern Nano-ZS90, UK). The surface morphology of the particles was

examined by a Hitachi S-3700N scanning electron microscope (SEM, Hitachi S-3700N, Japan). The surface functional groups of the particles were analyzed using an FTIR spectrometer with a resolution of 4 cm^{-1} in the region of 4000 to 400 cm^{-1}. An X-ray diffractometer (Y-2000, Dandong, China) equipped with Cu-Kα radiation was used to analyze the crystalline phase of particles. Elemental analysis of the biochars was carried out by an elemental analyzer (Vario el cube, Elementar, Germany).

Column experiments

Thereafter, the sand was washed with 15 pore volume (PV) of background solution circulated using a dual-channel peristaltic pump (HL-2, Chunding, Shanghai, China) to reduce the background value and endow the collector with a uniform and stable surface charge. Next, 15 PV of the selected concentrations of the particle solutions was pumped downwards through the column at a certain velocity (0.11 mL/s). To minimise particle aggregation and sedimentation, the suspensions were sonicated and continuously mixed at 250 r/min to maintain their homogeneity. A certain volume of effluent was digested with hydrochloric acid at a fixed time and finally analyzed with atomic absorption spectroscopy (AAS, Thermo Scientific iCE3500, USA). The breakthrough curves were plotted as normalized concentrations (C/C_0), computed as the ratio of measured effluent concentration (C) and the measured influent concentration (C_0), as a function of PV. The same experiment was repeated to investigate the transfer characteristics of bare-nZVI as well.

After the transport experiments, the spatial distribution of BC@nZVI in the column was studied. The end accessory was uninstalled, and the sand from the columns was sectioned at 2 cm intervals and carefully extruded into a 50-mL plastic centrifuge tubes. The sand in each centrifuge tube was digested with 1 M of HCl for 24 h and analyzed for total Fe by means of AAS. In this manner, the retention profiles (RPs) were drawn in terms of the content (M/M_{total}, M: mass of the particles retained in each section of the column; M_{total}: total mass of the particles recovered in the entire column) as a function of distance from the column inlet.

Experimental set-up

Sacrificial experiments were carried out according to our previous study (Wu et al., 2016). BDE 209 extraction method is based on our previous study (Wu et al., 2016).

The BDE209 concentrations in the extracts were identified by using a high-performance liquid chromatograph (Shimadzu, HP1100) equipped with a Phenomenon C18 column (250 mm × 4.6 mm) and a UV detector (SPD-10AV) operated at 240 nm. HPLC detection conditions were determined based on previous study (Wu et al., 2016).

Debromination efficiency were according to our previous study (Wu et al., 2016).

The specific formula is as follows Eq. (1):

$$Y_{Br^-}(\%) = \frac{[Br^-]_t / 80}{([BDE209]_0 / 959.17) \times 10} \times 100, \quad (1)$$

Where, the concentration unit of $[Br^-]_t$ is (mg/L) and $[BDE209]_0$ is (mg/L).

Appendix A3: FTIR analysis

The vibrations of aromatic –CH groups were observed for R-BC, W-BC and C-BC at the wavenumbers of 714.49–899.52 cm^{-1}, indicating the presence of adjacent aromatic hydrogen (Ahmad et al., 2012). The signals at 1115.1 cm^{-1} and 1031.4 cm^{-1} for R-BC and C-BC, respectively, were assigned to the C–O functional groups. The peaks near 1400 cm^{-1} represented the aromatic ring modes, which were present in the W-BC and C-BC samples. The peaks at approximately 1560 cm^{-1} (R-BC and C-BC) and 1620 cm^{-1} (B-BC and B-BC@nZVI) corresponded to the stretch vibrations of C=C and C=O, respectively. Notably, the clear bands at 3200–3550 cm^{-1} appeared only for B-BC. These bands are associated with -OH stretching and hydroxyl functional stretching vibrations, indicating the presence of hydroxyl groups on the surface of the B-BC samples (Wang et al., 2013). In short, the results suggested that the biochars were rich in organic functional groups. Moreover, the intense adsorption band in the B-BC@nZVI spectrum at 566.5 cm^{-1}, as shown in Fig. 1(f), indicated that an Fe–O bond was formed between BC and nZVI (Liu et al., 2010; Cazetta et al., 2016). However, there were a few significant differences between the FTIR spectra of B-BC and B-BC@nZVI. For example, a considerably lower absorption intensity was observed at approximately 3400 cm^{-1} and 1630 cm^{-1} in the case of B-BC@nZVI, which was potentially attributed to the reaction between nZVI and biochar. The results described above were confirmed by the XRD spectra.

Appendix A4: Kinetic analysis

It was known that the kinetics of removal of halogenated organic compounds by nZVI could be fitted best to a first-order kinetics model, as expressed by the following Eq. (2):

$$\frac{C_t}{C_0} = \exp\left(-k_{obs} t\right), \quad (2)$$

where C_t denotes the BDE209 concentration at the selected times (mg/L); C_0 the initial BDE209 concentration (mg/L); t the time (min or h) and k_{obs} the observed rate constant. The values of k_{obs} were calculated by means of linear regression by using Eq. (3):

$$Ln\frac{C_t}{C_0} = -k_{obs}t \quad , \qquad (3)$$

Table S1 Physicochemical properties of the soil used in this study

Soil property	Value
pH (1:2.5 soil to H_2O ratio)	5.83
Moisture content (%)	1.42
Cation exchange capacity (cmol/kg)	15.50
BDE209 (mg/kg)	Not detected
Ni (mg/kg) (Acid digestion)	Not detected
Available Fe (mg/kg) (DTPA)	118.66
Organic matter (g/kg)	65.49
Available P (mg/kg)	9.72

Table S2 Characteristics of the biochar samples

Biochar type	pH	Organic matter (g/kg)	Specific surface area (m^2/g)	Total pore volume (cm^3/g)	Elemental composition (wt.%)			
					C	H	N	S
Bagasse (B-BC)	10.05 ± 0.08	830 ± 5	352.6	0.154	79.3	3.14	0.55	0.42
Wood chips (W-BC)	9.24 ± 0.22	592 ± 5	42.1	0.014	56.8	3.79	0.28	0.32
Corn stalks (C-BC)	9.03 ± 0.04	552 ± 3	38.9	0.050	70.2	3.57	1.60	0.23
Rice straw (R-BC)	10.86 ± 0.20	625 ± 0.2	171.5	0.074	51.0	2.98	0.76	0.35

Table S3 Overview of the experimental values of Boxlucas1 fitting for the composite materials tested

Biochar type	BC:nZVI mass ratio	K_{obs} (h^{-1})	R^2
B-BC	0.11:1	0.18001	0.9602
B-BC	0.25:1	0.1584	0.9855
B-BC	0.5:1	0.1788	0.9698
B-BC	1:1	0.1884	0.9746
B-BC	1.5:1	0.1840	0.9660
B-BC	3:1	0.1834	0.9820
nZVI	0:1	0.0863	0.9802
W-BC	1:1	0.0996	0.9876
R-BC	1:1	0.1031	0.9937
C-BC	1:1	0.0882	0.9828

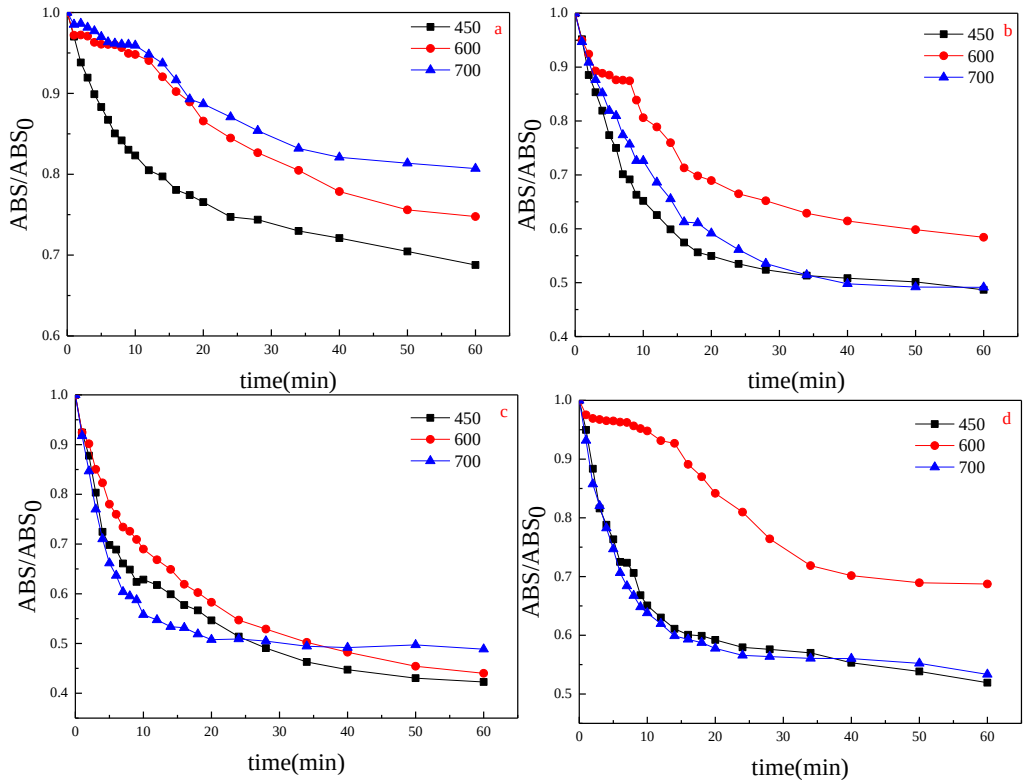

Fig. S1 Sedimentation tests of four BC@nZVI composites at different biochar pyrolysis temperatures: (a) B-BC@nZVI, (b) W-BC@nZVI, (c) R-BC@nZVI, (d) C-BC@nZVI

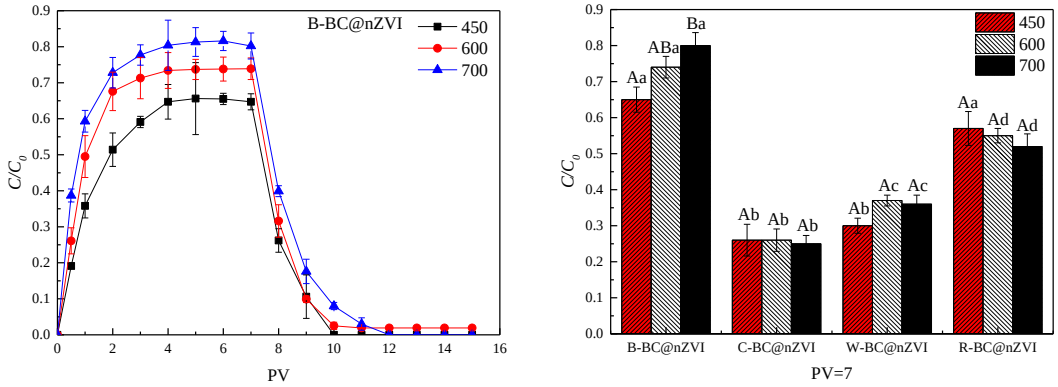

Fig. S2 (a) Breakthrough curves of B-BC@nZVI composites at different biochar pyrolysis temperatures and (b) relative concentration of four BC@nZVI composites at different biochar pyrolysis temperatures with PV=7

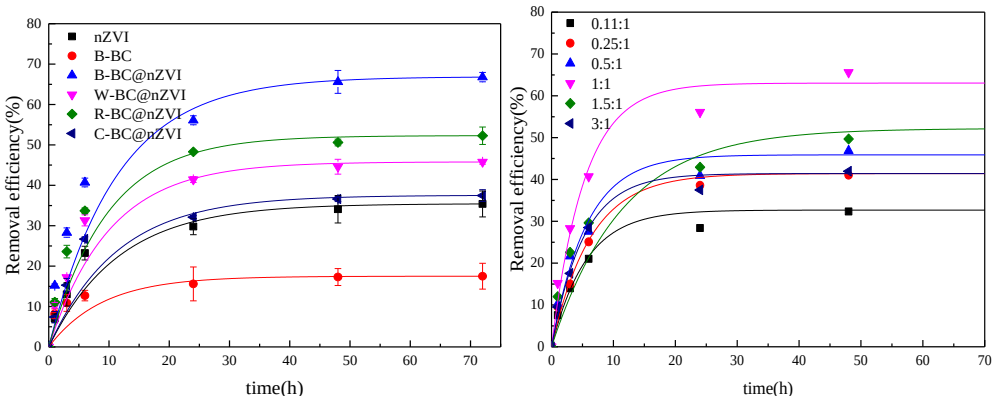

Fig. S3 BoxLucas1 fitting curves of (a) four BC@nZVI composites (b) B-BC@nZVI at different BC:nZVI mass ratios

References

Ahmad M, Lee S S, Dou X, Mohan D, Sung J K, Yang J E, Ok Y S (2012). Effects of pyrolysis temperature on soybean stover- and peanut shell-derived biochar properties and TCE adsorption in water. Bioresource Technology, 118: 536–544

Cazetta A L, Pezoti O, Bedin K C, Silva T L, Paesano A Junior, Asefa T, Almeida V C (2016). Magnetic activated carbon derived from biomass waste by concurrent synthesis: efficient adsorbent for toxic dyes. ACS Sustainable Chemistry & Engineering, 4(3): 1058–1068

Liu Z, Zhang F S, Wu J (2010). Characterization and application of chars produced from pinewood pyrolysis and hydrothermal treatment. Fuel, 89(2): 510–514

Wang Z, Zheng H, Luo Y, Deng X, Herbert S, Xing B (2013). Characterization and influence of biochars on nitrous oxide emission from agricultural soil. Environmental Pollution, 174: 289–296

Wu J, Yi Y, Li Y, Fang Z, Tsang E P (2016). Excellently reactive Ni/Fe bimetallic catalyst supported by biochar for the remediation of decabromodiphenyl contaminated soil: Reactivity, mechanism, pathways and reducing secondary risks. Journal of Hazardous Materials, 320: 341–349